Fluctuation theorem for heat transport probed by a thermal probe electrode

Y. Utsumi
Department of Physics Engineering, Faculty of Engineering, Mie University, Tsu, Mie, 514-8507, Japan

O. Entin-Wohlman and A. Aharony
Physics Department, Ben Gurion University, Beer Sheva 84105, Israel
and Raymond and Beverly Sackler School of Physics and Astronomy, Tel Aviv University, Tel Aviv 69978, Israel

T. Kubo and Y. Tokura
Graduate School of Pure and Applied Sciences, University of Tsukuba, Tsukuba, Ibaraki 305-8571, Japan
(Received 21 March 2014; published 22 May 2014)

We analyze the full-counting statistics of the electric heat current flowing in a two-terminal quantum conductor whose temperature is probed by a third electrode ("probe electrode"). In particular we demonstrate that the cumulant-generating function obeys the fluctuation theorem in the presence of a constant magnetic field. The analysis is based on the scattering matrix of the three-terminal junction (comprising the two electronic terminals and the probe electrode), and a separation of time scales: it is assumed that the rapid charge transfer across the conductor and the rapid relaxation of the electrons inside the probe electrode give rise to much slower energy fluctuations in the latter. This separation allows for a stochastic treatment of the probe dynamics, and the reduction of the three-terminal setup to an effective two-terminal one. Expressions for the lowest nonlinear transport coefficients, e.g., the linear-response heat-current noise and the second nonlinear thermal conductance, are obtained and explicitly shown to preserve the symmetry of the fluctuation theorem for the two-terminal conductor. The derivation of our expressions, which is based on the transport coefficients of the three-terminal system explicitly satisfying the fluctuation theorem, requires full calculations of vertex corrections.

DOI: 10.1103/PhysRevB.89.205314 PACS number(s): 05.30.−d, 72.70.+m, 73.63.Kv

I. INTRODUCTION

The recent progress in research in thermometry [1], refrigeration [2], and heating [3] processes in mesoscopic quantum systems enables one to treat systematically heat-related phenomena concerning electrons [4–7]. Recent efforts are focused on thermoelectric transport in coherent quantum conductors coupled to local vibrational modes [8], or to temperature- and/or potential-probing electrodes [9–11], in the linear-response regime and also beyond it [12–14]. An intriguing question raised in these investigations is the symmetry of the various transport coefficients with respect to time-reversal-symmetry breaking, in particular under the effect of inelastic interactions induced by probing electrodes. This question is further related to the fluctuation theorem (FT) obeyed by the cumulant-generating function.

The prototypical setup of coherent thermoelectric transport is a mesoscopic conductor connected to leads kept at various temperatures and a common chemical potential. For clarity, we focus below on a conductor coupled to two electronic reservoirs held at two (different) temperatures T_L and T_R. Broken time-reversal invariance is induced by a perpendicular magnetic field B, which affects the orbital motion of the electrons (the much smaller effect of the Zeeman interaction is disregarded). Our aim is to investigate the statistics of the heat current flowing in the conductor. The conductor is further coupled to a third electrode, designed to measure its temperature (see Fig. 1) [15,16]. This measurement is accomplished by adjusting the temperature T_P of this third terminal so that no net energy is flowing between it and the conductor on the average. However, the energy current flowing in or out of the probe electrode fluctuates in time and its distribution depends on details of the coupling between the quantum conductor and the probe (e.g., it is Poissonian for tunnel coupling). The fluctuations give rise to stochastic variations in the temperature of the probe. These in turn affect the higher cumulants (beyond the first two, i.e., the current and the noise) and the probability distribution of the energy current flowing between the two electronic reservoirs, i.e., the full-counting statistics (FCS) [17,18]. The problem at hand is therefore to find the cumulant-generating function (CGF) which characterizes this FCS, in the presence of the temperature-measuring probe electrode. In other words, we want to obtain the CGF once the three-terminal setup (where all three electrodes are included on equal footing) is mapped onto an effective two-terminal one in which energy is flowing between the left (L) and the right (R) reservoirs (see Fig. 1). An ensuing issue is the fate of the FT (imposed on the CGF) under this mapping, in particular when time-reversal invariance is broken.

A similar situation has been encountered in the statistics of charge currents. There, one has to allow for voltage-measuring probes (electrodes whose potential is adjusted so as to bar electric currents between them and the conductor) or dephasing probes (which exchange electrons incoherently with the conductor within a narrow energy interval). The treatment of the stochastic effects of these electrodes on the CGF is based on time scale separation. For example, the rapid flow of electrons in and out of a voltage-probing electrode results in much slower charge fluctuations there, thus allowing for a stochastic path integration of the CGF of the full setup (e.g., a three-terminal one) over all configurations of the probe charge, to obtain the reduced CGF of the physical setup (e.g., a two-terminal one) [19–22]. A similar treatment has

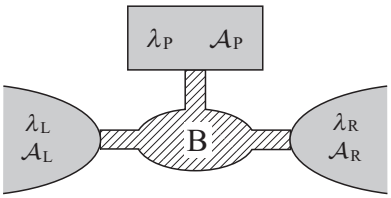

FIG. 1. A three-terminal setup. The figure depicts a quantum conductor (the elliptical area) connected to two reservoirs denoted L and R, which are held at two different temperatures; those are expressed in terms of the affinities $\mathcal{A}_{L,R} \equiv \beta - \beta_{L,R}$ (β^{-1} is the temperature of the entire system when at equilibrium); see the text. The thermal probe (the upper square) is specified by its own affinity $\mathcal{A}_P \equiv \beta - \beta_P$, which fluctuates in time. Also shown are the three auxiliary "counting" fields λ_r ($r = L$, R, and P) which measure the energy flowing in and out of electrode r. The quantum conductor is threaded by a perpendicularly oriented magnetic field B. Once the stochastic dynamics of the energy current in and out of the probe electrode is taken care of, the junction becomes an effective two-terminal one.

been carried out for the stochastic temperature and chemical potential fluctuations in an overheated metallic island [23–25].

However, to the best of our knowledge there are no studies of the fluctuation theorem [26–43] in systems coupled to thermal probes. This paper is devoted to the exploration of this issue. In order to map the three-terminal junction of Fig. 1 onto an effective two-terminal one we adopt the stochastic path-integral formalism [19–22], originally devised for describing electric conduction through a chaotic cavity. We analyze the FT pertaining to the resulting effective two-terminal setup. In particular we investigate the symmetry relations of the nonlinear thermal conductances and the linear-response expressions for the corresponding noise correlations and verify that those obey the universal relations imposed by the FT [30]. Explicit results for the aforementioned energy-transport coefficients are presented by using a triple-quantum-dot junction as an example. It allows us to demonstrate the magnetic-field asymmetry induced in the heat transport by the thermal probe (see, e.g., Ref. [44] for related issues), and to confirm that the universal relations imposed by the FT are satisfied.

The FT is a consequence of microreversibility and can be considered as a microscopic extension of the second law of thermodynamics. It can be expressed in terms of the probability distribution $P_\tau(\Delta S)$ for an entropy change ΔS during a measurement time τ. When time-reversal invariance is broken, say by a magnetic field B, that probability distribution depends on the latter as well, and the FT reads

$$\lim_{\tau\to\infty} \frac{1}{\tau} \ln \frac{P_\tau(\Delta S; B)}{P_\tau(-\Delta S; -B)} = I_S, \tag{1}$$

where $I_S = \lim_{\tau\to\infty} \Delta S/\tau$ is the entropy flow. In a two-terminal junction coupled to two electronic reservoirs held at the same chemical potential but at different temperatures T_L and T_R, this flow is [45]

$$I_S = I_E(\beta_R - \beta_L), \tag{2}$$

where I_E is the energy current, and where β denotes the inverse temperature. (We use units in which $e = \hbar = k_B = 1$ and measure energies from the common chemical potential $\mu = 0$, thus ensuring that the electronic heat current is equivalent to the energy current [45].) The direction of the current flow here is out of each electrode [46].

Despite its modest form, the FT Eq. (1) is a very powerful relation. It reproduces the linear-response results, the fluctuation-dissipation theorem, and Onsager's reciprocal relations [27–33]. Furthermore, it predicts universal relations among the nonlinear transport coefficients [28–31]. A recent experiment has aimed to verify some of these relations [38], by comparing the nonlinear conductance of an Aharonov-Bohm interferometer with the noise in the linear-response regime.

The paper is organized as follows. We begin in Sec. II by setting the formal basis of the paper: First we summarize in Sec. II A the probability distribution of the energy currents carried by noninteracting electrons across a quantum conductor connected to three terminals (i.e., left, right, and probe electrodes) and its CGF, together with the symmetries implied by the FT. Then, in Sec. II B, following the same route taken in Refs. [19–25], we path-integrate over the stochastic energy fluctuations in the probe and thus reduce the three-terminal setup to an effective two-terminal one. We continue in Sec. II C by proving that this reduction is consistent with the FT as applied to the reduced two-terminal setup; this is the first main result of this paper. In Sec. II D we consider the scaled two-terminal CGF at steady state. We continue in Sec. III A by introducing the general scheme for obtaining the transport coefficients when time-reversal symmetry is broken. Then in Sec. III B we explain how the transport coefficients of the effective two-terminal junction are obtained from the CGF of the three-terminal one, and introduce the required vertex corrections. This analysis allows us to obtain in Sec. III C the lowest nonlinear transport coefficients; this is the second main result of this paper. Finally in Sec. III D we apply our theory to the three-terminal triple-quantum-dot system. Our results are summarized in Sec. IV.

II. FULL-COUNTING STATISTICS

A. Cumulant-generating function for a quantum conductor coupled to three terminals

Figure 1 displays our system schematically: A quantum conductor whose temperature (T_P) is determined by a thermal probe, is subject to a magnetic field B and is attached to two electronic reservoirs (of temperatures T_L and T_R). This three-terminal setup is specified by a 3×3 energy- and magnetic-field-dependent scattering matrix $\mathbf{S}(\omega; B)$, whose elements are the various scattering amplitudes. Those obey microreversibility,

$$S_{rr'}(\omega; B) = S_{r'r}(\omega; -B), \tag{3}$$

with $r,r' = L$, R, or P. Each of the three terminals is specified by a Fermi distribution at its own temperature,

$$f_r(\omega) = [e^{\beta_r\omega} + 1]^{-1} = [e^{(\beta-\mathcal{A}_r)\omega} + 1]^{-1}. \tag{4}$$

In the second equality of Eq. (4) we have introduced the affinity $\mathcal{A}_r$ corresponding to the rth reservoir,

$$\mathcal{A}_r = \beta - \beta_r, \tag{5}$$

where β denotes the common inverse temperature of the entire junction. These affinities, sometimes called "thermodynamic forces," drive the energy currents in the junction.

The statistical properties of the energy transfer are characterized by the probability distribution of the three energy currents I_{Er} emerging from each electrode. Alternatively, one may exploit the probability distribution $P_{G\tau}(\{\varepsilon_r\})$ of the energies accumulated on the three electrodes during the measurement time τ,

$$\varepsilon_r \equiv \int_0^\tau dt\, I_{Er}(t). \tag{6}$$

The probability distribution $P_{G\tau}(\{\varepsilon_r\})$ is also a function of B. (For brevity, the explicit dependencies of some of the functions below are suppressed in part of the equations and are presented when needed for clarity.) The (scaled) cumulant-generating function $\mathcal{F}_G$ defined in the limit of long measurement times is

$$\mathcal{F}_G(\{\lambda_r\}) = \lim_{\tau\to\infty} \frac{1}{\tau} \ln \mathcal{Z}_{G\tau}(\{\lambda_r\}), \tag{7}$$

where $\mathcal{Z}_{G\tau}$ is the Fourier transform of the probability $P_{G\tau}(\{\varepsilon_r\})$ for a finite measurement time τ:

$$\mathcal{Z}_{G\tau}(\{\lambda_r\}) = \int_{-\infty}^{\infty} d\varepsilon_L d\varepsilon_R d\varepsilon_P e^{i\sum_r \varepsilon_r\lambda_r} P_{G\tau}(\{\varepsilon_r\}). \tag{8}$$

We may now examine the symmetries imposed by the FT Eq. (1) on the CGF $\mathcal{F}_G$. The entropy production $\dot{S}$, which in our case is equivalent to the energy current, is given by

$$\dot{S} = \sum_{r=L,R,P} I_{Er}(\beta - \beta_r) = \sum_{r=L,R,P} I_{Er}\mathcal{A}_r, \tag{9}$$

where in the last step we have used Eq. (5). It therefore follows that $\Delta S = \sum_r \varepsilon_r \mathcal{A}_r$ and consequently, in the limit of long measurement times $\tau \to \infty$, the FT takes the familiar form

$$P_{G\tau}(\{\varepsilon_r\}; B) = P_{G\tau}(\{-\varepsilon_r\}; -B) e^{\sum_r \varepsilon_r \mathcal{A}_r}. \tag{10}$$

This, in turn, implies that the CGF obeys [28–30]

$$\mathcal{F}_G(\{\lambda_r\},\{\mathcal{A}_r\}; B) = \mathcal{F}_G(\{-\lambda_r + i\mathcal{A}_r\},\{\mathcal{A}_r\}; -B). \tag{11}$$

Here we stress that the probability distribution $P_{G\tau}$ is for the three-terminal system including the probe terminal. As such, it is still an intermediate expression. Later, in Eq. (21), we present the two-terminal probability distribution P_τ after removing the probe terminal. $P_{G\tau}$ and P_τ are different and should not be confused.

A convenient way to express and calculate the CGF of the energy current [47] for *noninteracting electrons* is in terms of the scattering matrix $\mathbf{S}(\omega; B)$

$$\mathcal{F}_G(\{\lambda_r\}) = \int \frac{d\omega}{2\pi} \ln\det[\mathbf{1} - \mathbf{f}(\omega)\mathbf{K}(\boldsymbol{\lambda},\omega; B)], \tag{12}$$

with the matrix $\mathbf{K}$ given by

$$\mathbf{K}(\boldsymbol{\lambda},\omega; B) = 1 - e^{i\boldsymbol{\lambda}\omega}\mathbf{S}^\dagger(\omega; B) e^{-i\boldsymbol{\lambda}\omega}\mathbf{S}(\omega; B). \tag{13}$$

In Eqs. (12) and (13), $\mathbf{f}$ is a diagonal matrix of the Fermi functions,

$$\mathbf{f}(\omega) = \mathrm{diag}\{f_L(\omega), f_R(\omega), f_P(\omega)\}, \tag{14}$$

and $\boldsymbol{\lambda}$ is a diagonal matrix comprising the counting fields

$$\boldsymbol{\lambda} = \mathrm{diag}\{\lambda_L,\lambda_R,\lambda_P\}. \tag{15}$$

Obviously, the CGF in its form (12) should obey [29] the FT relation Eq. (11) (see Appendix A for details).

B. Stochastic treatment of the probe energy

Here we outline the stochastic approach which allows for the path integration over the slow dynamics of the energy in the probe electrode, and leads to a functional representation for the CGF of the effective two-terminal junction [20]. As is mentioned above, the temperature of the probe fluctuates in time, i.e., the probe affinity $\mathcal{A}_P$ is time dependent and consequently so is the (instantaneous) probe energy denoted $E(t)$, which is given by

$$E(t) = \int d\omega \rho_P(\omega) \frac{\omega}{e^{[\beta - \mathcal{A}_P(t)]\omega} + 1}, \tag{16}$$

where ρ_P is the electronic density of states in the probe. The energy $E(t)$ fluctuates stochastically since the energy current generated by the electrons in the quantum conductor fluctuates. Such energy-current fluctuations result in non-Gaussian white noise, whose rigorous stochastic calculus has been investigated recently [48]. In the present paper we adopt a simpler approximation which captures the relevant physics [19–25]. This approach relies on the existence of two distinct time scales. The faster one pertains to the traveling time of each electron through the conductor and the subsequent relaxation in any of the electrodes. The slower one is related to the fluctuations of the energy inside the probe terminal.

During a time interval Δt, the energy emitted stochastically from the rth electrode is

$$\Delta\varepsilon_r = \int_t^{t+\Delta t} dt'\, I_{Er}(t'). \tag{17}$$

These energy differences obey a joint probability distribution governed by the scaled CGF [see Eqs. (7) and (8)]

$$P_{G\Delta t}(\{\Delta\varepsilon_r\},\{\mathcal{A}_r\}; B) = \int_{-\infty}^{\infty} \frac{d\lambda_L d\lambda_R d\lambda_P}{(2\pi)^3} e^{\Delta t \mathcal{F}_G(\{\lambda_r\},\{\mathcal{A}_r\}; B) - i\sum_r \Delta\varepsilon_r\lambda_r}. \tag{18}$$

However, the time interval Δt is chosen in a specific manner designed to single out $\Delta\varepsilon_P$ and to make it a stochastic variable. Indeed, the key approximation in Refs. [19–25] is related to the duration of Δt. It should be longer than the time needed for the probe electrode to reach local equilibrium, which is obviously much longer than the time scale characterizing the energy fluctuations in the probe. In other words, Δt is much longer than the time required for an electron to relax in the probe electrode. The latter time scale is determined for example by electron-electron collisions (the probe electrode is in the hot-electron regime).

One next discretizes the entire measurement time τ into $N = \tau/\Delta t$ intervals, each of duration Δt. When the probe energy at time $t_n = n\Delta t$ is E_n, then after an additional time step it changes to

$$E_{n+1} = E_n + \Delta\varepsilon_P. \tag{19}$$

Since $\Delta\varepsilon_P$ is a stochastic variable, E_{n+1} is not unique. By using the probability distribution of $\Delta\varepsilon_P$, Eqs. (18) and (19), we obtain the conditional joint probability of finding the probe energy E_n at time $t = t_n$ and E_{n+1} at $t = t_{n+1} = (n+1)\Delta t$, accompanied by the energy changes $\Delta\varepsilon_{Ln}$ and $\Delta\varepsilon_{Rn}$ of the left and right reservoirs

$$P_{G\Delta t}(\Delta\varepsilon_{Ln},\Delta\varepsilon_{Rn},E_{n+1}-E_n,\mathcal{A}_L,\mathcal{A}_R,\mathcal{A}_P([E_{n+1}+E_n]/2);B), \tag{20}$$

where we have assumed that during Δt the probe affinity is determined by Eq. (16) with the average energy at times t_{n+1} and t_n, $\mathcal{A}_P([E_{n+1}+E_n]/2)$. Although from the viewpoint of causality it would be more reasonable to use instead $\mathcal{A}_P(E_n)$, this midpoint rule is convenient for proving the FT (see Sec. II C).

It follows from the above that only two adjacent events determine the probe dynamics, making it a Markov process. Hence, the probability distribution for the energies $\varepsilon_{L/R} = \sum_{j=0}^{N-1}\Delta\varepsilon_{L/Rj}$ to emerge from the left and right reservoirs during the measurement time τ is

$$\begin{aligned}P_\tau(\varepsilon_L,\varepsilon_R,\mathcal{A}_L,\mathcal{A}_R;B) = \int\left(\prod_{j=0}^{N-1}d\Delta\varepsilon_{Lj}d\Delta\varepsilon_{Rj}\right)\left(\prod_{j=0}^{N}dE_j\right)\delta\left(\varepsilon_L-\sum_{j=0}^{N-1}\Delta\varepsilon_{Lj}\right)\delta\left(\varepsilon_R-\sum_{j=0}^{N-1}\Delta\varepsilon_{Rj}\right)\\ \times P_{G\Delta t}(\Delta\varepsilon_{LN-1},\Delta\varepsilon_{RN-1},E_N-E_{N-1},\mathcal{A}_L,\mathcal{A}_R,\mathcal{A}_P([E_N+E_{N-1}]/2);B)\cdots\\ \times P_{G\Delta t}(\Delta\varepsilon_{L0},\Delta\varepsilon_{R0},E_1-E_0,\mathcal{A}_L,\mathcal{A}_R,\mathcal{A}_P([E_1+E_0]/2);B)\,p_P(E_0).\end{aligned} \tag{21}$$

Here $p_P(E_0)$ is the equilibrium distribution probability of the probe energy at an initial time t_0. The second and third lines of the right-hand side of Eq. (21) express the probability of finding a path in energy space $E_0,E_1,\ldots,E_N$, at $t_0,t_1,\ldots,t_N$. The characteristic function is the Fourier transform of Eq. (21),

$$\begin{aligned}\mathcal{Z}_\tau(\{\lambda_r\},\{\mathcal{A}_r\};B) &= \int d\varepsilon_L d\varepsilon_R e^{i\lambda_L\varepsilon_L+i\lambda_R\varepsilon_R}P_\tau(\{\epsilon_r\},\{\mathcal{A}_r\};B)\\ &= \int\left(\prod_{j=0}^{N-1}\frac{d\lambda_{Pj}}{2\pi}\prod_{j=0}^{N}dE_j\right)p_P(E_0)e^{-i\sum_{j=0}^{N-1}\lambda_{Pj}(E_{j+1}-E_j)+\sum_{j=0}^{N-1}\Delta t\mathcal{F}_G(\lambda_L,\lambda_R,\lambda_{Pj},\mathcal{A}_L,\mathcal{A}_R,\mathcal{A}_P([E_{j+1}+E_j]/2);B)},\end{aligned} \tag{22}$$

where now the arguments $\{\lambda_r\}$ and $\{\mathcal{A}_r\}$ refer to the counting fields and affinities of solely the left and right electronic reservoirs.

In the continuum limit $\Delta t\to 0$, the characteristic function becomes

$$\mathcal{Z}_\tau(\{\lambda_r\},\{\mathcal{A}_r\};B) = \int\mathcal{D}[\lambda_P,E]\,e^{i\mathcal{S}}p_P(E(0))\,, \tag{23}$$

where $\int\mathcal{D}[\lambda_P,E]$ means functional integration over $\lambda_P(t)$ and $E(t)$. The Martin-Siggia-Rose action [23,24,49] $\mathcal{S}$ is given by

$$i\mathcal{S} = -\int_0^\tau dt[i\lambda_P(t)\dot{E}(t) - \mathcal{F}_G(\lambda_L,\lambda_R,\lambda_P(t),\mathcal{A}_L,\mathcal{A}_R,\mathcal{A}_P(E(t));B)]. \tag{24}$$

C. Fluctuation theorem for the reduced two-terminal system

The probability distribution of the effective two-terminal junction, Eq. (21), is based on the assumption that the dynamics of the energy flow in and out of the probe is slow and can be treated stochastically. Therefore, it is not *a priori* obvious that the CGF thus derived obeys the fluctuation theorem. Here we prove that it does.

The proof begins with Eqs. (10) and (20) which yield the extended form of the local detailed balance [50] or the detailed fluctuation theorem [51],

$$\begin{aligned}&P_{G\Delta t}\{\Delta\varepsilon_{Lj-1},\Delta\varepsilon_{Rj-1},E_j-E_{j-1},\mathcal{A}_L,\mathcal{A}_R,\mathcal{A}_P([E_j+E_{j-1}]/2);B\}\\ &\quad= P_{G\Delta t}(-\Delta\varepsilon_{Lj-1},-\Delta\varepsilon_{Rj-1},E_{j-1}-E_j,\mathcal{A}_L,\mathcal{A}_R,\mathcal{A}_P([E_{j-1}+E_j]/2);-B)e^{\sum_{r=L,R}\Delta\varepsilon_{rj-1}\mathcal{A}_r}p_P(E_j)/p_P(E_{j-1})\,.\end{aligned} \tag{25}$$

Here we have imposed the first law of thermodynamics for the fluctuating energy,

$$\mathcal{A}_P((E_{j+1}+E_j)/2)(E_{j+1}-E_j) = \ln p_P(E_{j+1}) - \ln p_P(E_j) + O(\Delta t^2), \tag{26}$$

and introduced the instantaneous equilibrium probability $p_P(E_j)$ to find the probe energy E_j at time t_j. It then follows from Eq. (21) that

$$\begin{aligned}P_\tau(\{\varepsilon_r\},\{\mathcal{A}_r\};B) = \int\left(\prod_{j=0}^{N-1}d\Delta\varepsilon_{Lj}d\Delta\varepsilon_{Rj}\right)\left(\prod_{j=0}^{N}dE_j\right)\delta\left(\varepsilon_L-\sum_{j=0}^{N-1}\Delta\varepsilon_{Lj}\right)\delta\left(\varepsilon_R-\sum_{j=0}^{N-1}\Delta\varepsilon_{Rj}\right)\\ \times e^{\sum_{j=0}^{N-1}(\Delta\varepsilon_{Lj}\mathcal{A}_L+\Delta\varepsilon_{Rj}\mathcal{A}_R)}P_{\Delta t}(-\Delta\varepsilon_{L0},-\Delta\varepsilon_{R0},E_0-E_1,\mathcal{A}_L,\mathcal{A}_R,\mathcal{A}_P([E_0+E_1]/2);-B)\cdots\end{aligned}$$

$$\times P_{\Delta t}(-\Delta\varepsilon_{LN-1}, -\Delta\varepsilon_{RN-1}, E_{N-1}-E_N, \mathcal{A}_L, \mathcal{A}_R, \mathcal{A}_P([E_{N-1}+E_N]/2); -B)\, p_P(E_N)$$
$$= P_\tau(\{-\varepsilon_r\},\{\mathcal{A}_r\}; -B) e^{\varepsilon_L \mathcal{A}_L + \varepsilon_R \mathcal{A}_R}, \quad r = L, R. \tag{27}$$

Upon Fourier-transforming this expression, one finds that the characteristic function obeys the fluctuation theorem,

$$\mathcal{Z}_\tau(\{\lambda_r\},\{\mathcal{A}_r\}; B) = \mathcal{Z}_\tau(\{-\lambda_r + i\mathcal{A}_r\},\{\mathcal{A}_r\}; -B), \tag{28}$$

similarly to Eq. (10). Thus we have demonstrated that the stochastic path-integral treatment of the temperature probe is consistent with the FT. This proof, which is similar to the one given [52] for the work fluctuation theorem of an LC circuit coupled to a quantum conductor [53], is one of the main results of our paper.

D. The steady state

To perform the functional integral of Eq. (23), we adopt the saddle-point approximation [19], for which $\delta\mathcal{S}/\delta(i\lambda_P(t)) = \delta\mathcal{S}/\delta E(t) = 0$, and consequently

$$\dot{E} = \frac{\partial \mathcal{F}_G}{\partial(i\lambda_P)}, \quad i\dot{\lambda}_P = -\frac{\partial \mathcal{F}_G}{\partial E}. \tag{29}$$

These equations are analogous to Hamilton's equations of motion if $i\lambda_P$ is regarded as the "momentum," E as the "coordinate," and $\mathcal{F}_G$ as the "Hamiltonian" (see Sec. IV in Ref. [49]). When $\lambda_L = \lambda_R = 0$, a steady-state solution satisfying $\dot{\lambda}_P = \dot{E} = 0$ corresponds to a saddle-point of the "Hamiltonian" residing on the E axis satisfying $i\lambda_P = 0$. However, for $\lambda_L, \lambda_R \neq 0$, which we are considering in the present paper, it is not the case. It is convenient to use $\mathcal{A}_P$ instead of E by using Eq. (16). Then Eqs. (29) can be rewritten as

$$T_P^2\, C_P\, \dot{\mathcal{A}}_P = \frac{\partial \mathcal{F}_G}{\partial(i\lambda_P)}, \quad T_P^2\, C_P\, i\dot{\lambda}_P = -\frac{\partial \mathcal{F}_G}{\partial \mathcal{A}_P}. \tag{30}$$

Here $T_P \equiv (\beta - \mathcal{A}_P)^{-1}$ is the (finite) probe temperature and $C_P = \partial E/\partial T_P$ is its heat capacitance. Therefore, when the heat capacitance C_P is finite, a steady state can be reached and corresponding solutions λ_P^* and $\mathcal{A}_P^*$ (which are purely imaginary and purely real, respectively) can be calculated from

$$\frac{\partial}{\partial \lambda_P^*}\mathcal{F}_G(\lambda_L,\lambda_R,\lambda_P^*,\mathcal{A}_L,\mathcal{A}_R,\mathcal{A}_P^*; B)$$
$$= \frac{\partial}{\partial \mathcal{A}_P^*}\mathcal{F}_G(\lambda_L,\lambda_R,\lambda_P^*,\mathcal{A}_L,\mathcal{A}_R,\mathcal{A}_P^*; B) = 0\,. \tag{31}$$

The scaled CGF of the two-terminal junction,

$$\mathcal{F}(\{\lambda_r\},\{\mathcal{A}_r\}; B) = \lim_{\tau\to\infty} \frac{\ln \mathcal{Z}_\tau(\{\lambda_r\},\{\mathcal{A}_r\}; B)}{\tau}, \tag{32}$$

is then related to that of the three-terminal junction upon using in the expression for the latter the saddle-point approximation values

$$\mathcal{F}(\{\lambda_r\},\{\mathcal{A}_r\}; B) = \mathcal{F}_G(\lambda_L,\lambda_R,\lambda_P^*,\mathcal{A}_L,\mathcal{A}_R,\mathcal{A}_P^*; B). \tag{33}$$

Equation (33) is a large-deviation function [54], which maximizes the probability of finding zero net current through the probe electrode by properly choosing $\mathcal{A}_P$. The characteristic function is then approximately given by $\mathcal{Z}_\tau \approx \exp(\tau\mathcal{F})$.

As a consequence of energy conservation, the two-terminal scaled CGF (33) is a function of only the *difference* between the left and the right counting fields, $\lambda = \lambda_L - \lambda_R$. To see this, we return to the three-terminal scaled CGF Eq. (12) and note that, again as a result of energy conservation, it is invariant under a common shift of the three counting fields,

$$\lambda_r \to \lambda_r + \delta\lambda. \tag{34}$$

This means that it can be expressed as a function of *two* counting fields. In addition, λ_P is a "floating" variable determined by the saddle-point condition Eq. (31), which means that a shift of λ_P alone,

$$\lambda_P \to \lambda_P + \delta\lambda_P, \tag{35}$$

cannot change the scaled CGF belonging to the effective two-terminal junction.

Taking advantage of the invariance under the shifts Eqs. (34) and (35), and rewriting the three-terminal CGF as a function of two independent counting fields λ and λ_P and the corresponding two affinities $\mathcal{A}$ and $\mathcal{A}_P$, we obtain

$$\mathcal{F}_G(\lambda,\lambda_P,\mathcal{A},\mathcal{A}_P; B, x)$$
$$\equiv \mathcal{F}_G[(1+x)\lambda, x\lambda, \lambda_P, (1+x)\mathcal{A}, x\mathcal{A}, \mathcal{A}_P; B]. \tag{36}$$

Here we have introduced the parameter x, which measures the asymmetry in the inverse-temperature drop between the left and right electrodes,

$$\mathcal{A}_L = (1+x)\,\mathcal{A}, \quad \mathcal{A}_R = x\,\mathcal{A}. \tag{37}$$

(This parameter is dictated by the details of the experimental setup.) Note that the form Eq. (36) for the CGF of the three-terminal setup satisfies the FT,

$$\mathcal{F}_G(\lambda,\lambda_P,\mathcal{A},\mathcal{A}_P; B, x)$$
$$= \mathcal{F}_G(-\lambda + i\mathcal{A}, -\lambda_P + i\mathcal{A}_P, \mathcal{A}, \mathcal{A}_P; -B, x). \tag{38}$$

The second advantage of Eq. (36) is that it can be used to simplify the saddle-point condition. By shifting the counting fields, $\lambda_r \to \lambda_r - \lambda_R + x\lambda$, Eq. (31) becomes

$$\frac{\partial}{\partial \lambda_P^*}\mathcal{F}_G(\lambda,\lambda_P^* - \lambda_R + x\lambda,\mathcal{A},\mathcal{A}_P^*; B, x)$$
$$= \frac{\partial}{\partial \mathcal{A}_P^*}\mathcal{F}_G(\lambda,\lambda_P^* - \lambda_R + x\lambda,\mathcal{A},\mathcal{A}_P^*; B, x) = 0, \tag{39}$$

and consequently, upon choosing $\lambda_P^* \to \lambda_P^* - \lambda_R + x\lambda$, we obtain

$$\frac{\partial}{\partial \lambda_P^*}\mathcal{F}_G(\lambda,\lambda_P^*,\mathcal{A},\mathcal{A}_P^*; B, x)$$
$$= \frac{\partial}{\partial \mathcal{A}_P^*}\mathcal{F}_G(\lambda,\lambda_P^*,\mathcal{A},\mathcal{A}_P^*; B, x) = 0. \tag{40}$$

The corresponding CGF of the effective two-terminal junction is then

$$\mathcal{F}(\lambda,\mathcal{A}; B, x) = \mathcal{F}_G(\lambda,\lambda_P^*,\mathcal{A},\mathcal{A}_P^*; B, x), \tag{41}$$

which depends on a single counting field λ. The two-terminal FT Eq. (28) can now be expressed as

$$\mathcal{F}(\lambda,\mathcal{A};B,x)=\mathcal{F}(-\lambda+i\mathcal{A},\mathcal{A};-B,x). \tag{42}$$

Equations (40) and (41) are the starting point of the following calculations.

III. TRANSPORT COEFFICIENTS AND VERTEX CORRECTIONS

A. Transport coefficients

Once the CGF Eq. (41) is found, the various cumulants are obtained upon differentiating it with respect to the counting field and the affinity,

$$\left\langle\!\left\langle \delta I_E^j \right\rangle\!\right\rangle = \left.\frac{\partial^j \mathcal{F}(\lambda,\mathcal{A};B,x)}{\partial(i\lambda)^j}\right|_{\lambda=0} = \sum_{k=0}^{\infty} L_k^j \frac{\mathcal{A}^k}{k!}, \tag{43}$$

where the transport coefficients of the reduced two-terminal junction are given by

$$L_k^j \equiv \left.\frac{d^{j+k}\mathcal{F}}{d(i\lambda)^j d\mathcal{A}^k}\right|_{\lambda=\mathcal{A}=0}. \tag{44}$$

For example, L_1^1 corresponds to the linear-response thermal conductivity, while L_0^2 is its noise in equilibrium.

In the presence of a magnetic field, it is convenient to introduce symmetrized/antisymmetrized forms of the transport coefficients,

$$L_{k,\pm}^j = L_k^j(B) \pm L_k^j(-B). \tag{45}$$

By combining the two-terminal FT (42) with the definition (44) one obtains certain universal relations among the nonlinear transport coefficients L_j^i, which are valid out of equilibrium [30]. Relevant relations are summarized in Appendix B.

In Sec. III B we express the two-terminal transport coefficients using those of the three-terminal junction. The latter are derivatives of the CGF Eq. (36),

$$L_{km}^{j\ell}(B) \equiv \left.\frac{\partial^{j+k+\ell+m}\mathcal{F}_G}{\partial(i\lambda)^j\partial\mathcal{A}^k\partial(i\lambda_P)^\ell\partial\mathcal{A}_P^m}\right|_{\lambda=\lambda_P=\mathcal{A}=\mathcal{A}_P=0}. \tag{46}$$

By combining the three-terminal FT (38) with the definition (46), one obtains certain universal relations among the nonlinear transport coefficients $L_{j\ell}^{ik}$, which are also summarized in Appendix B.

There is a subtle point related to the choice of the "coordinates," i.e., the counting fields and the affinities (see Appendix C). As discussed above, the three-terminal transport coefficients are invariant under shifts of the counting fields Eqs. (34) and (35). This redundancy results in different but equivalent expressions for the two-terminal transport coefficients. The situation is similar to what happens in the presence of gauge fields, where different choices of the gauge result in apparently different expressions, which are, in fact, identical. Previous research has exploited the minimal-correlation coordinate [20] (see Appendix C), which simplifies drastically the calculations at the price of expressions which do not explicitly obey the FT and consequently miss symmetries among the transport coefficients.

B. Vertex corrections

While the procedure outlined above for determining the transport coefficients of the effective two-terminal junction is seemingly straightforward, it is not free of certain pitfalls. As can be seen from the left-hand side of Eq. (41), small variations of the counting field and affinity of the two-terminal junction, λ and $\mathcal{A}$, lead to small shifts in the saddle-point values of the counting field and affinity of the probe, λ_P^* and $\mathcal{A}_P^*$. These shifts, in turn, give rise to corrections in the transport coefficients of the two-terminal junction, i.e., vertex corrections [see Eq. (57) below]. Here we outline the derivation of the first few cumulants, taking into account these vertex corrections. Technically, the procedure we follow is identical to the one performed in the self-consistent Φ-derivable approximation [55,56] and the saddle-point approximation in the Schwinger-Keldysh path-integral approach [39].

In order to keep the equations compact, we introduce the shorthand notations $a_c=\mathcal{A}, a_q=i\lambda$, and $v_c=\mathcal{A}_P, v_q=i\lambda_P$. In terms of these, the saddle-point equations (40) become

$$\partial\mathcal{F}_G/\partial v_\alpha = 0, \tag{47}$$

where $\alpha=c,q$. The complete derivative of Eq. (47) with respect to a_γ ($\gamma=c,q$) is

$$\frac{d}{da_\gamma}\frac{\partial\mathcal{F}_G}{\partial v_\alpha} = \frac{\partial^2\mathcal{F}_G}{\partial v_\alpha\partial a_\gamma} + \sum_{\alpha'=c,q}\frac{\partial^2\mathcal{F}_G}{\partial v_\alpha\partial v_{\alpha'}}\frac{dv_{\alpha'}}{da_\gamma} = 0. \tag{48}$$

It therefore follows that

$$\frac{dv_\alpha}{da_\gamma} = \sum_{\alpha'=c,q} U_{\alpha\alpha'}\frac{\partial^2\mathcal{F}_G}{\partial a_\gamma\,\partial v_{\alpha'}}, \tag{49}$$

where the matrix U obeys

$$\sum_{\alpha'=c,q} U_{\alpha\alpha'}\frac{\partial^2\mathcal{F}_G}{\partial v_{\alpha'}\partial v_{\alpha''}} = -\delta_{\alpha\alpha''}, \quad U_{\alpha\alpha''}=U_{\alpha''\alpha}. \tag{50}$$

Furthermore, the partial derivatives of U are given by

$$\begin{aligned}\frac{\partial U_{\alpha\alpha'}}{\partial a_{\alpha''}} &= \sum_{\gamma,\gamma'=c,q} U_{\alpha\gamma}\frac{\partial^3\mathcal{F}_G}{\partial a_{\alpha''}\,\partial v_\gamma\,\partial v_{\gamma'}}U_{\gamma'\alpha'},\\ \frac{\partial U_{\alpha\alpha'}}{\partial v_{\alpha''}} &= \sum_{\gamma,\gamma'=c,q} U_{\alpha\gamma}\frac{\partial^3\mathcal{F}_G}{\partial v_{\alpha''}\,\partial v_\gamma\,\partial v_{\gamma'}}U_{\gamma'\alpha'},\end{aligned} \tag{51}$$

which can be verified by differentiating the first of Eqs. (50).

We can now obtain the first derivative of the CGF of the two-terminal junction in terms of derivatives of the CGF of the three-terminal one,

$$\frac{d\mathcal{F}}{da_\gamma} = \frac{\partial\mathcal{F}_G}{\partial a_\gamma} + \sum_{\alpha=c,q}\frac{\partial v_\alpha}{\partial a_\gamma}\frac{\partial\mathcal{F}_G}{\partial v_\alpha} = \frac{\partial\mathcal{F}_G}{\partial a_\gamma}, \tag{52}$$

where we have used Eq. (47). To obtain the second derivative, we completely differentiate Eq. (52),

$$\begin{aligned}\frac{d^2\mathcal{F}}{da_{\gamma'}\,da_\gamma} &= \frac{\partial^2\mathcal{F}_G}{\partial a_{\gamma'}\,\partial a_\gamma} + \sum_{\alpha=c,q}\frac{dv_\alpha}{da_{\gamma'}}\frac{\partial^2\mathcal{F}_G}{\partial a_\gamma\,\partial v_\alpha}\\ &= \frac{\partial^2\mathcal{F}_G}{\partial a_{\gamma'}\,\partial a_\gamma} + \sum_{\alpha,\alpha'=c,q}\frac{\partial^2\mathcal{F}_G}{\partial a_{\gamma'}\,\partial v_\alpha}U_{\alpha\alpha'}\frac{\partial^2\mathcal{F}_G}{\partial a_\gamma\,\partial v_{\alpha'}},\end{aligned} \tag{53}$$

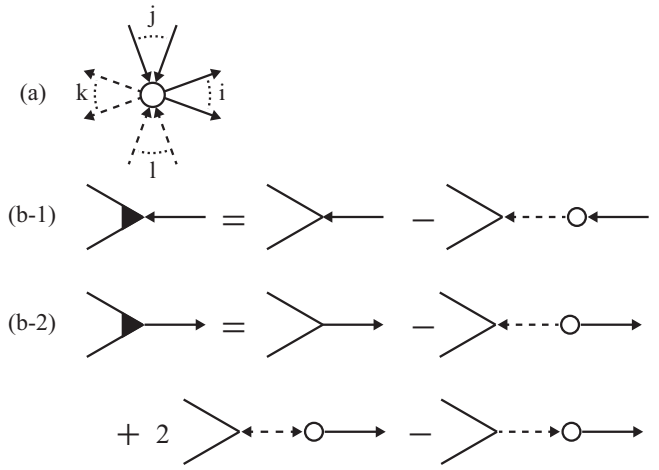

FIG. 2. (a) A bare vertex (empty circle) $L^{ik}_{j\ell}$; (b1) and (b2) corrected vertices (solid triangles).

where we have used Eq. (49). Note that the final form is symmetric in a_γ and $a_{\gamma'}$. The third derivative can be obtained by further differentiating Eq. (53). The lengthy expression of the third derivative is relegated to Appendix D.

The derivatives of the CGF of the two-terminal junction given in Eqs. (52), (53), and (D1) indicate the explicit form of the vertex corrections: the full derivative is obtained upon inserting

$$\frac{d}{da_\gamma} \to \frac{\partial}{\partial a_\gamma} + \sum_{\alpha'=c,q} \frac{\partial^2 \mathcal{F}_G}{\partial v_{\alpha'} \partial a_\gamma} U_{\alpha'\alpha} \frac{\partial}{\partial v_\alpha} \tag{54}$$

into each bare vertex. Let us now explore these vertex corrections in detail. Note that in deriving the transport coefficients one has to set $\lambda = \mathcal{A} = 0$ after performing the differentiations [see Eq. (44)]. Under these circumstances the saddle-point solution is $\lambda_P^* = \mathcal{A}_P^* = 0$, and consequently the matrix U, Eq. (50), becomes

$$U \to -\left[\begin{array}{cc} \frac{\partial^2 \mathcal{F}_G}{\partial \mathcal{A}_P \partial \mathcal{A}_P} & \frac{\partial^2 \mathcal{F}_G}{\partial \mathcal{A}_P \partial (i\lambda_P)} \\ \frac{\partial^2 \mathcal{F}_G}{\partial (i\lambda_P) \partial \mathcal{A}_P} & \frac{\partial^2 \mathcal{F}_G}{\partial (i\lambda_P) \partial (i\lambda_P)} \end{array}\right]^{-1}\Bigg|_{\lambda=\lambda_P=\mathcal{A}=\mathcal{A}_P=0}$$
$$= \frac{1}{L^{01}_{01,+}} \begin{bmatrix} 2 & -1 \\ -1 & 0 \end{bmatrix}. \tag{55}$$

The last equality here is obtained upon using Eqs. (B10) and (B11). Similarly, the matrix $\partial^2 \mathcal{F}_G / \partial v_k \partial a_i$ is

$$\left[\begin{array}{cc} \frac{\partial^2 \mathcal{F}_G}{\partial \mathcal{A}_P \partial \mathcal{A}} & \frac{\partial^2 \mathcal{F}_G}{\partial \mathcal{A}_P \partial (i\lambda)} \\ \frac{\partial^2 \mathcal{F}_G}{\partial (i\lambda_P) \partial \mathcal{A}} & \frac{\partial^2 \mathcal{F}_G}{\partial (i\lambda_P) \partial (i\lambda)} \end{array}\right]\Bigg|_{\lambda=\lambda_P=\mathcal{A}=\mathcal{A}_P=0} = \begin{bmatrix} 0 & L^{10}_{01} \\ L^{01}_{10} & L^{11}_{00} \end{bmatrix}. \tag{56}$$

Collecting these results, Eq. (54) can be written explicitly as (for $\lambda = \lambda_P = \mathcal{A} = \mathcal{A}_P = 0$)

$$\begin{aligned} \frac{d}{d\mathcal{A}} &\to \frac{\partial}{\partial \mathcal{A}} - \frac{L^{01}_{10}}{L^{01}_{01,+}} \frac{\partial}{\partial \mathcal{A}_P}, \\ \frac{d}{d(i\lambda)} &\to \frac{\partial}{\partial (i\lambda)} + \frac{2L^{10}_{01} - L^{11}_{00}}{L^{01}_{01,+}} \frac{\partial}{\partial \mathcal{A}_P} - \frac{L^{10}_{01}}{L^{01}_{01,+}} \frac{\partial}{\partial (i\lambda_P)}. \end{aligned} \tag{57}$$

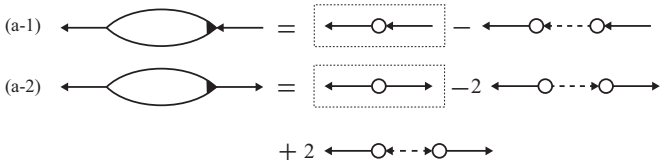

FIG. 3. Diagrams for the linear-response conductance (a1) and the equilibrium noise (a2). Only the "bare" diagrams, indicated by dotted squares, are included in the minimal-correlation coordinate approach explained in Appendix C.

Following Ref. [57] the vertex corrections can be visualized diagrammatically. Figure 2(a) depicts a "bare" vertex, connecting i outgoing solid lines, k outgoing dotted lines, j incoming solid lines, and ℓ incoming dotted lines which correspond to $L^{ik}_{j\ell}$. The dressed vortices presented in Eqs. (57) are shown in Figs. 2(b1) and 2(b2), respectively.

C. Linear and lowest nonlinear transport coefficients

Here we exploit the general formulas derived in Sec. III B to present expressions for the transport coefficients of the heat current in the linear-response regime, and the lowest nonlinear ones. Figures 3(a1) and 3(a2) portray the diagrams for the linear-response conductance and the equilibrium noise, respectively, leading to the expressions [see Eq. (44)]

$$\begin{aligned} L^2_0/2 = L^1_1 = L^{10}_{10,+} - \frac{\left(L^{10}_{01,+}\right)^2 - \left(L^{01}_{10,-}\right)^2}{L^{01}_{01,+}}, \\ L^{10}_{10,-} = 0, \end{aligned} \tag{58}$$

which satisfy the fluctuation-dissipation theorem and the Onsager relations [see Eqs. (B6) and (B7) and the discussion around them]. Furthermore, by Eqs. (C3) and (C6), Eqs. (58) reproduce the well-known result (see, e.g., Ref. [46] for the electric-transport analog),

$$L^1_1 = K_{LL} - \frac{K_{LP} K_{PL}}{K_{PP}}, \tag{59}$$

where K_{ab} are the elements of the three-terminal heat-conductance matrix defined in Eq. (C2).

There are six vertex-correction diagrams comprising the lowest nonlinear conductance; these are shown in Fig. 4, leading to the expression

$$\begin{aligned} L^1_2 = L^{10}_{20} - \frac{L^{10}_{01} L^{01}_{20} + 2L^{01}_{10} L^{10}_{11}}{L^{01}_{01}} \\ + \frac{\left(L^{01}_{10}\right)^2 L^{10}_{02} + 2L^{01}_{10} L^{10}_{01} L^{01}_{11}}{\left(L^{01}_{01}\right)^2} - \frac{\left(L^{01}_{10}\right)^2 L^{10}_{01} L^{01}_{02}}{\left(L^{01}_{01}\right)^3}. \end{aligned} \tag{60}$$

One notes the appearance of the second nonlinear thermal conductances of the three-terminal junction, $L^{10}_{11} L^{10}_{02}$, L^{01}_{20}, L^{01}_{11}, and L^{01}_{02}, which enter this expression because of the changes in the temperature of the probe electrode. However, as can be seen from Eq. (12), the simultaneous derivatives of the CGF with respect to $\mathcal{A}$ and $\mathcal{A}_P$ vanish,

$$L^{10}_{11} = L^{01}_{11} = 0, \tag{61}$$

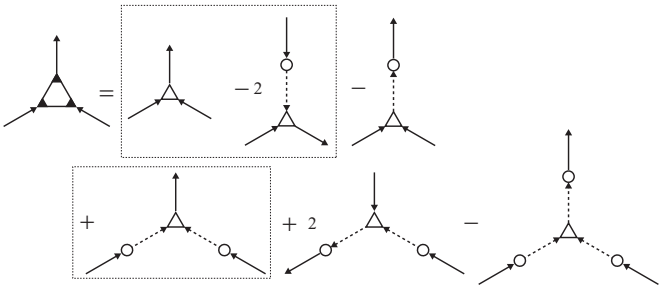

FIG. 4. The six diagrams comprising the second nonlinear conductance. The three diagrams enclosed in the dotted squares are the bare one and its cascade corrections, which are accounted for in the minimal-correlation coordinate approach (Appendix C). The second and fifth diagrams on the right-hand side contain L_{11}^{10} and L_{11}^{01}, respectively, and thus vanish.

and therefore Eq. (60) is simplified,

$$L_2^1 = L_{20}^{10} - \frac{L_{01}^{10}L_{20}^{01}}{L_{01}^{01}} + \frac{\left(L_{10}^{01}\right)^2 L_{02}^{10}}{\left(L_{01}^{01}\right)^2} - \frac{\left(L_{10}^{01}\right)^2 L_{01}^{10}L_{02}^{01}}{\left(L_{01}^{01}\right)^3}. \tag{62}$$

The expression for the linear-response noise results from the diagrams depicted in Fig. 5 and turns out to be rather complicated even after utilizing Eq. (61). However, by using the universal relations among the bare transport coefficients of the three-terminal junction, Eqs. (B12), it is possible to show that the components symmetric with respect to a magnetic field and the antisymmetric ones obey

$$\begin{aligned} L_{2,+}^1 &= L_{1,+}^2, \\ L_{2,-}^1 &= L_{1,-}^2/3. \end{aligned} \tag{63}$$

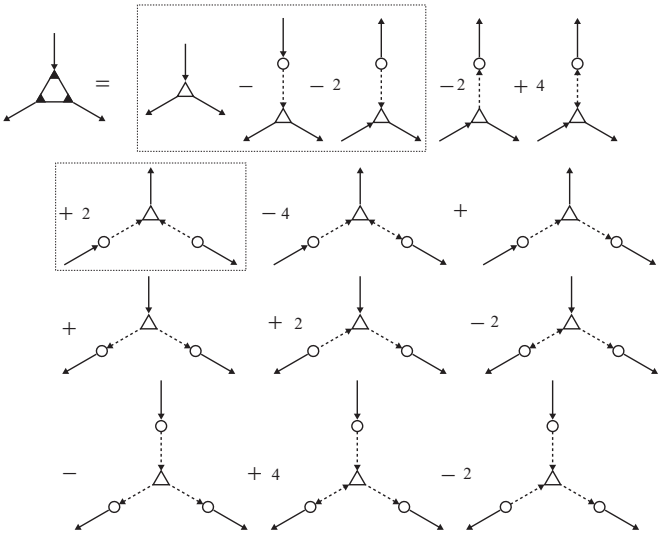

FIG. 5. The 14 diagrams contributing to the expression for the linear-response noise. The four diagrams enclosed in the dotted squares are accounted for in the minimal-correlation coordinate approach (Appendix C). The third and fifth diagrams on the right-hand side contain L_{11}^{10} and the 10th and the 11th ones contain L_{11}^{01}. These diagrams therefore vanish.

[See Eqs. (E1) and (E2) for the explicit expressions.] These relations between the noise in the linear-response regime and the second nonlinear conductance agree with the universal relations derived in Ref. [30] [see Eqs. (B8)].

The number of the diagrams is reduced considerably when one adopts the approach of the minimal-correlation coordinate [20]; see Appendix C and in particular Eq. (C7). Then, only three (four) diagrams remain for the second nonlinear conductance (the linear-response noise) as indicated by dotted squares in Fig. 4 (Fig. 5). This is obviously advantageous for practical use, e.g., for a numerical calculation. However, since the bare three-terminal transport coefficients do not satisfy the universal relations presented in Appendix B, it is not possible to prove the symmetry of Eq. (63) analytically [it is possible for our case as given in Eqs. (E1) and (E2)], which is, in our opinion, a weak point.

D. Three-terminal triple quantum dot

The general results presented in the previous sections are explicitly illustrated in this section by analyzing a triple quantum dot connected to three terminals and threaded by a magnetic flux $\Phi = Bs$, as shown schematically in Fig. 6(a) (s is the relevant area). The system is described by the Hamiltonian

$$\begin{aligned} \mathcal{H} = &\sum_{j=1}^{3} \epsilon_0 d_j^\dagger d_j + \sum_{j=1}^{3}\sum_{k} \epsilon_k a_{jk}^\dagger a_{jk} \\ &+ \sum_{j=1}^{3}\left(t e^{i\phi/3} d_{j+1}^\dagger d_j + \sum_k t_{jk} d_j^\dagger a_{jk} + \text{H.c} \right), \end{aligned} \tag{64}$$

where for simplicity the spin degree of freedom is ignored. The first term in Eq. (64) pertains to the three uncoupled dots (with each dot represented by a single energy level); the second describes the three electrodes (assuming each to consist of a free electron gas. To make the expression compact we identify the left, right, and probe electrodes with the first, second, and third electrodes, respectively, and the third gives the tunneling between neighboring dots and between each dot and the electrode to which it is attached. In Eq. (64), d_j annihilates an electron on the jth dot (with $d_4 \equiv d_1$), a_{jk} destroys an electron with wave vector k in the jth electrode, t is the hopping matrix element between adjacent dots, and t_{jk} is the tunneling matrix element between the jth dot and jth electrode. The effect of a magnetic field is contained in the Aharonov-Bohm phase $\phi = \Phi/\Phi_0$, where $\Phi_0 = \hbar c/e$ is the flux quantum; hence ϕ reverses its sign when $B \to -B$.

The scattering matrix of the triple-quantum-dot system comprises the following elements:

$$\begin{aligned} S_{j+1\,j}(\omega; B) &= \{4e^{-i\phi/3} t\Gamma[\Gamma - 2i(\omega - \epsilon_0 + te^{i\phi})]\}/\Delta(\phi), \\ S_{j\,j+1}(\omega; B) &= S_{j+1\,j}(\omega; -B), \\ S_{jj}(\omega; B) &= \{[2(\omega - \epsilon_0) - i\Gamma][2(\omega - \epsilon_0) + i\Gamma]^2 \\ &\quad - 4t^2[6(\omega - \epsilon_0) + i\Gamma] - 16t^3 \cos\phi\}/\Delta(\phi), \end{aligned} \tag{65}$$

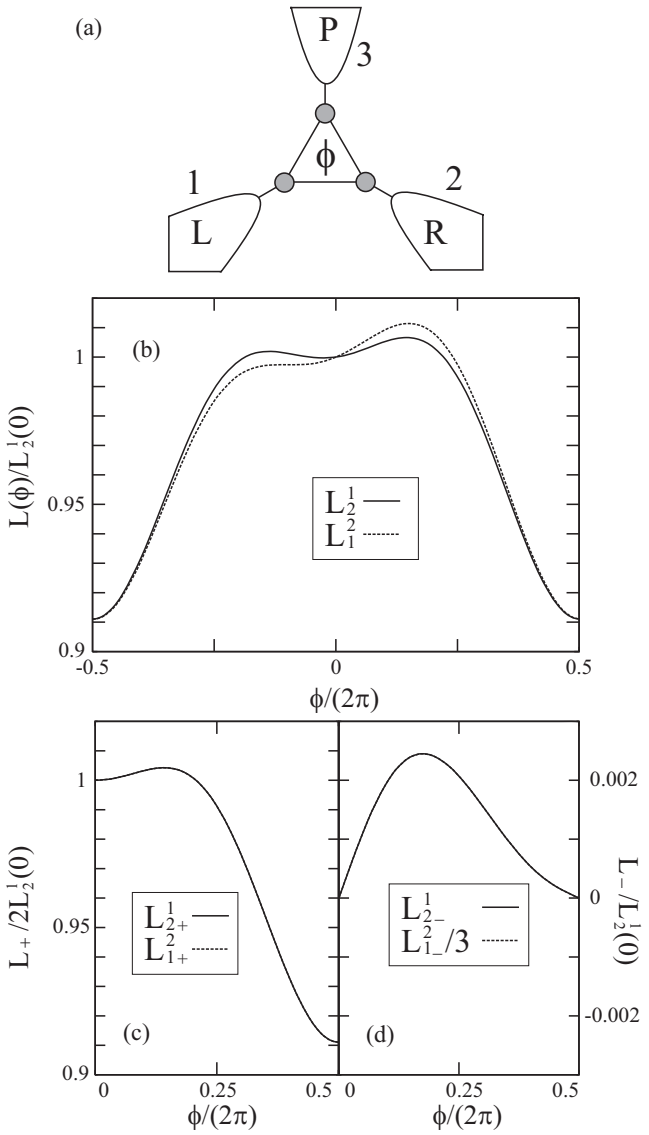

FIG. 6. (a) Schematic picture of three-terminal triple quantum dot. The flux threads the triangular region. (b) The second nonlinear thermal conductance (solid line) and the linear-response thermal noise (dotted line) as functions of the flux. $L_2^1(0) = 1.39 \times 10^{-4}\Gamma^3/(e^2 R_K)$, where $R_K = h/e^2$ is the resistance quantum. (c) and (d) show the symmetric (solid lines) and antisymmetric (dashed lines) components in the flux. Solid and dashed lines in each panel overlap each other. Parameters: $t = 0.1\Gamma$, $\epsilon_0 = -0.5\Gamma$, $\beta\Gamma = 10$, and $x = 0.25$.

where

$$\Delta(\phi) = [2(\omega - \epsilon_0) + i\Gamma]^3 - 12\,t^2[2(\omega - \epsilon_0) + i\Gamma] - 16\,t^3\cos\phi. \tag{66}$$

We have assumed here that the tunnel coupling strength is energy independent and introduced the level broadening

$$\Gamma = 2\pi \sum_k |t_{jk}|^2 \delta(\omega - \epsilon_k). \tag{67}$$

Figure 6(b) shows the flux dependence of the second nonlinear thermal conductance L_2^1 (solid line) and the linear-response expression for the heat-current noise L_1^2 (dotted line). As can be seen, the curves are not symmetric with respect to the flux ϕ. Such an antisymmetric component induced by the magnetic field at out-of-equilibrium conditions is absent for the two-terminal conductor of noninteracting electrons, but is finite for the setup with a probe (for the magnetic-field-induced electric heat-current asymmetry, see e.g. Ref. [44]). From Fig. 6(b), we may conclude that L_2^1 (solid line) and L_1^2 (dotted line) are uncorrelated. However, when we look at the symmetrized and the antisymmetrized components [defined in Eq. (45)] the correlation becomes clearer. Figure 6(c) shows the symmetrized components $L_{2,+}^1$ (solid line) and $L_{1,+}^2$ (dotted line). Figure 6(d) shows the antisymmetrized components (with 1/3 for the linear response of noise) $L_{2,-}^1$ (solid line) and $L_{1,-}^2/3$ (dotted line). The two panels show that the solid lines and the dotted lines overlap, which means that the FT Eq. (63) is satisfied.

A recent study of the Langevin equation with non-Gaussian white noise suggests that non-Gaussian corrections around the saddle point play a crucial role in certain cases [48]. We have therefore checked numerically that the saddle-point solution provides a physically reasonable probability distribution in the case of the triple dot. In the limit of long measurement times τ, the inverse Fourier transform of the characteristic function can be written approximately as a Legendre-Fenchel transform of the scaled CGF (32),

$$P_\tau(\{\epsilon_r\},\{\mathcal{A}_r\};B) = \frac{1}{2\pi}\int d\lambda e^{-i\lambda\varepsilon_L + \tau\mathcal{F}(\lambda,\mathcal{A};B,x)}\delta(\varepsilon_L + \varepsilon_R) \approx e^{-\tau\mathcal{I}}\,\delta(\varepsilon_L + \varepsilon_R), \tag{68}$$

where ϵ_L and ϵ_R are electron energies flowing out of the left (first) electrode and the right(second) electrode, respectively. The cumulant-generating function $\mathcal{F}$ was given in Eq. (33) with the S matrix for the three-terminal triple quantum dot. $\mathcal{I}$ is the rate function [54]

$$\mathcal{I} = \max_\lambda\,[i\lambda I_E - \mathcal{F}(\lambda,\mathcal{A},;B,x)]\,, \tag{69}$$

with λ being a purely imaginary number. This result verifies that the heat current flowing out of the left junction and that flowing into the right junction are identical, $I_E = \lim_{\tau\to\infty}\varepsilon_L/\tau = \lim_{\tau\to\infty} -\varepsilon_R/\tau$.

Figure 7(a) depicts the rate function, calculated by numerically solving the saddle-point equations (40). This procedure yields a single solution and it results in a reasonable rate function as shown in Fig. 7(a). Furthermore, by using Eqs. (1) and (68), the FT in the limit of long measurement times can be expressed as $\mathcal{I}(-I_E) - \mathcal{I}(I_E) = I_E\mathcal{A}$. This equality is plotted in Fig. 7(b), which further supports the validity of our numerical solution.

IV. SUMMARY

We have investigated the fluctuation theorem of the heat transfer driven by a temperature difference across a three-terminal conductor for which one of the electrodes serves as a probe electrode used to measure the conductor temperature. The stochastic energy fluctuations in the probe electrode are integrated over to yield the cumulant-generating function of the reduced two-terminal junction. We have proven that this generating function satisfies the two-terminal fluctuation

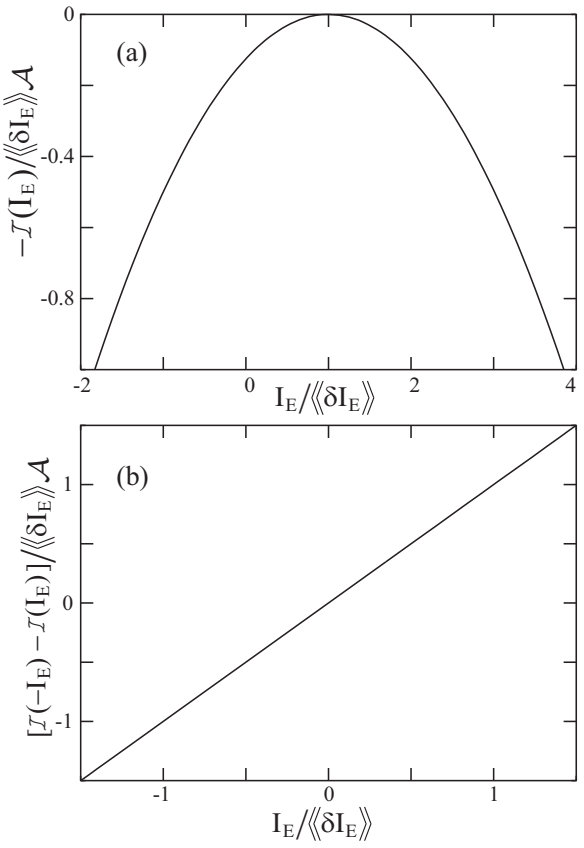

FIG. 7. (a) The rate function and (b) the fluctuation theorem for $\phi = 0$. Parameters: $\mathcal{A}\Gamma = 0.5$, $\beta\Gamma = 10$.

theorem. We have obtained expressions for the second nonlinear conductance and the linear-response noise, and have shown explicitly that they obey the symmetries imposed by the FT. Furthermore, we have shown that in order for this symmetries to hold, it is imperative to account for all vertex corrections entering the expressions for the transport coefficients. We stress that our expressions for the transport coefficients *explicitly* preserve the symmetry of the fluctuation theorem [Eqs. (E1) and (E2)], which is not the case for those drawn from the approach of the minimal-correlation coordinate [20]. We have applied our theory to a three-terminal triple-quantum-dot system.

We have included in our analysis solely the thermodynamic driving forces resulting from temperature differences. A full treatment of thermoelectricity requires the inclusion of chemical-potential gradients, as well as voltage probes; these will be handled in future presentations.

ACKNOWLEDGMENTS

We thank Dimitri Golubev, Hisao Hayakawa, and Kiyoshi Kanazawa for valuable discussions. This work was supported by a Grant-in-Aid for Young Scientists (B) (Grant No. 23740294), MEXT kakenhi "Quantum Cybernetics" (Grant No. 21102003), the Israeli Science Foundation (ISF), and the U.S.-Israel Binational Science Foundation (BSF). O.E.-W. and A.A. acknowledge gratefully the hospitality of Tsukuba University, where this work was completed.

APPENDIX A: PROOF OF THE FT FOR THE CGF IN TERMS OF THE SCATTERING MATRIX

In order to keep the paper self-contained, we outline in this appendix the proof that the CGF as given in terms of the scattering matrix $\mathbf{S}$ [see Eq. (12)] obeys the symmetries derived from the FT, i.e., Eq. (11). To this end we adopt the representation of the scattering matrix introduced in Refs. [17] and [29] (see Appendix A in the latter). For convenience of notation, we denote here the left ($r = L$), the right ($r = R$), and the probe ($r = P$) electrodes by 1, 2, and 3, respectively.

The first step is to decompose the determinant in the integrand of Eq. (12) into terms describing multiparticle scattering events by using the Cauchy-Binet formula,

$$\begin{aligned}\det[\mathbf{1}-\mathbf{f}(\omega)\mathbf{K}(\boldsymbol{\lambda},\omega;B)] &= \sum_I\sum_O \left|\mathbf{S}(\omega;B)^O_I\right|^2 \left(\prod_{r\in I,r'\notin I} f_r(1-f_{r'})\right)\exp\left(-i\sum_{s\in I}\lambda_s\omega + i\sum_{s'\in O}\lambda_{s'}\omega\right)\\ &= \sum_I\sum_O \left|\mathbf{S}(\omega;B)^O_I\right|^2 \left(\prod_r (1-f_r)\right)\exp\left(-i\sum_{s\in I}(\lambda_s - i\beta_s)\omega + i\sum_{s'\in O}\lambda_{s'}\omega\right). \end{aligned} \tag{A1}$$

Here I is a set of terminals from which particles are emerging, and O is the one in which they are being absorbed. For a three-terminal junction, $I, O = \{1,2,3\}$ or $I, O = \{1,2\},\{2,3\},\{1,3\}$, or $I, O = \{1\},\{2\},\{3\}$. The square matrix $\mathbf{S}^O_I$ is one of the submatrices of the scattering matrix $\mathbf{S}$ with rows O and columns I, and $|\mathbf{S}^O_I|$ is its determinant, i.e., it is the minor. For example, $I = \{2,3\}$ and $O = \{1,2\}$ means that particles are emerging from terminals R and P and are then absorbed in terminals L and R. The submatrix is then

$$\mathbf{S}^{\{1,2\}}_{\{2,3\}} = \begin{bmatrix} S_{LR} & S_{LP} \\ S_{RR} & S_{RP} \end{bmatrix}. \tag{A2}$$

Next, the transformation $\lambda_r \to -\lambda_r + i\mathcal{A}_r$ is applied to Eq. (A1) to yield

$$\begin{aligned}\det[\mathbf{1}-\mathbf{f}(\omega)\mathbf{K}(\boldsymbol{\lambda},\omega;B)] &\to \sum_I\sum_O \left|\mathbf{S}(\omega;B)^O_I\right|^2 \left(\prod_r (1-f_r)\right)\exp\left(i\sum_{s\in I}\lambda_s\omega - i\sum_{s'\in O}(\lambda_{s'} - i\beta_{s'})\omega\right)\\ &= \sum_I\sum_O \left|\mathbf{S}(\omega;-B)^O_I\right|^2 \left(\prod_r (1-f_r)\right)\exp\left(-i\sum_{s'\in O}(\lambda_{s'} - i\beta_{s'})\omega + i\sum_{s\in I}\lambda_s\omega\right)\\ &= \det[\mathbf{1}-\mathbf{f}(\omega)\mathbf{K}(\boldsymbol{\lambda},\omega;-B)], \end{aligned} \tag{A3}$$

where we have used the microreversibility condition Eq. (3). Equation (A3) proves that the CGF in its representation (12) (valid for noninteracting electrons) obeys the FT.

APPENDIX B: RELATIONS AMONG THE TRANSPORT COEFFICIENTS

The fluctuation theorem imposes certain relations among the transport coefficients [30]. Here we summarize several of them. In order to derive those one considers the symmetrized and antisymmetrized forms of the FT as applied to the two-terminal CGF,

$$\begin{aligned}&\mathcal{F}(\lambda,\mathcal{A};B,x)\pm\mathcal{F}(\lambda,\mathcal{A};-B,x)\\&\quad=\mathcal{F}(-\lambda+i\mathcal{A},\mathcal{A};-B,x)\pm\mathcal{F}(-\lambda+i\mathcal{A},\mathcal{A};B,x),\end{aligned}\tag{B1}$$

and the symmetrized and antisymmetrized coefficients

$$L^n_{m,\pm}(B)=L^n_m(B)\pm L^n_m(-B),\tag{B2}$$

where L^n_m is defined in Eq. (44). By expanding both sides of Eq. (B1) in powers of the counting field λ and the affinity $\mathcal{A}$ and comparing the resulting coefficients, it is found that

$$L^n_{m\pm}=\pm\sum_{k=0}^{m}\binom{m}{k}(-1)^{k+n}L^{n+k}_{m-k\,\pm}.\tag{B3}$$

The normalization of the CGF implies that $\mathcal{F}(0,\mathcal{A};B)=0$, and consequently

$$L^0_n=0.\tag{B4}$$

The lowest nontrivial coefficient, for which $m=n=1$, is [see Eq. (B3)]

$$L^1_{1\pm}=\pm\left(-L^1_{1\pm}+L^2_{0\pm}\right).\tag{B5}$$

This relation yields that the linear-response coefficients obey the fluctuation-dissipation theorem relating the linear-response thermal conductance to its noise,

$$L^1_{1+}=L^2_{0+}/2,\tag{B6}$$

and the Onsager relation imposing that the linear-response thermal conductance and also its noise are even in the magnetic field,

$$L^1_{1-}=L^2_{0-}=0.\tag{B7}$$

Similarly, Eqs. (B3) and (B4) produce interrelations among the coefficients which hold beyond linear response, e.g.,

$$\begin{aligned}L^1_{2+}&=L^2_{1+},\\L^1_{2-}&=L^2_{1-}/3=L^3_{0-}/6,\\L^3_{0+}&=0.\end{aligned}\tag{B8}$$

For completeness, we present below similar relations for a three-terminal junction. By using Eq. (38), these are determined by an expression analogous to Eq. (B3),

$$\begin{aligned}L^{n_1\,n_2}_{m_1\,m_2\pm}=\pm\sum_{k_1=0}^{m_1}\sum_{k_2=0}^{m_2}&\binom{m_1}{k_1}\binom{m_2}{k_2}\\&\times(-1)^{k_1+n_1+k_2+n_2}L^{n_1+k_1\,n_2+k_2}_{m_1-k_1\,m_2-k_2\pm}.\end{aligned}\tag{B9}$$

From this expression, in conjunction with the normalization condition $L^{00}_{m_1\,m_2\pm}=0$, one can obtain several classes of interrelations. First, there are those of the linear-response regime, which obey the fluctuation-dissipation theorem

$$\begin{aligned}L^{10}_{10,+}&=L^{20}_{00,+}/2,\\L^{01}_{01,+}&=L^{02}_{00,+}/2.\end{aligned}\tag{B10}$$

Second, there are the Onsager-Casimir relations,

$$\begin{aligned}&L^{10}_{01,+}=L^{01}_{10,+}=L^{11}_{00,+}/2,\\&L^{11}_{00,-}=0,\\&L^{10}_{01,-}=-L^{01}_{10,-},\\&L^{10}_{10,-}=L^{20}_{00,-}=L^{01}_{01,-}=L^{02}_{00,-}=0.\end{aligned}\tag{B11}$$

These symmetries are identical to those obtained for electrical transport [46]. Third, there are relations for the higher transport coefficients, beyond the linear-response regime,

$$\begin{aligned}&L^{30}_{00,+}=0,\\&L^{10}_{20,+}=L^{20}_{10,+},\\&L^{10}_{20,-}=L^{20}_{10,-}/3=L^{30}_{00,-}/6,\\&L^{03}_{00,+}=0,\\&L^{01}_{02,+}=L^{02}_{01,+},\\&L^{01}_{02,-}=L^{02}_{01,-}/3=L^{03}_{00,-}/6,\\&L^{21}_{00,+}=0,\\&L^{01}_{20,+}=L^{11}_{10,+}=2\,L^{10}_{11,+}-L^{20}_{01,+},\\&L^{20}_{01,-}=L^{11}_{10,-}=L^{21}_{00,-}/2=L^{01}_{20,-}+2\,L^{10}_{11,-},\\&L^{12}_{00,+}=0,\\&L^{10}_{02,+}=L^{11}_{01,+}=2\,L^{01}_{11,+}-L^{02}_{10,+},\\&L^{02}_{10,-}=L^{11}_{01,-}=L^{12}_{00,-}/2=L^{10}_{02,-}+2\,L^{01}_{11,-}.\end{aligned}\tag{B12}$$

APPENDIX C: THE MINIMAL-CORRELATION COORDINATE

Here we provide more explanations concerning the hidden redundancy in the expressions for the transport coefficients. A ubiquitous procedure to characterize the linear-response conductances of a three-terminal junction is to introduce a 3×3 conductance matrix $K_{rr'}$, in terms of which the energy currents are

$$I_{Er}=\sum_{r'}K_{rr'}\mathcal{A}_{r'}.\tag{C1}$$

The heat conductance matrix thus includes nine elements, but these are not independent. For example, when that matrix is derived from Eq. (12) upon using the identity $(d/dx)\ln\det\mathbf{M}=\mathrm{Tr}\{\mathbf{M}^{-1}d\mathbf{M}/dx\}$ (where $\mathbf{M}$ is an arbitrary

matrix), one finds

$$K_{rr'} = \left.\frac{\partial^2 \mathcal{F}_G(\{\lambda_r\},\{\mathcal{A}_r\};B)}{\partial \mathcal{A}_{r'}\partial(i\lambda_r)}\right|_{\lambda_r=\mathcal{A}_r=0} = \frac{1}{4\pi}\int d\omega\,\omega^2\,\frac{\delta_{rr'}-|S_{rr'}(\omega;B)|^2}{1+\cosh(\beta\omega)}. \tag{C2}$$

From the unitarity of the scattering matrix **S** it follows that

$$\sum_r K_{rr'} = \sum_{r'} K_{rr'} = 0, \tag{C3}$$

and therefore the nine components of **K** are not independent. The transport coefficients as introduced in Eq. (46) are free of redundancies and provide compact expressions.

There are many ways to remove the above-mentioned redundancies. For example, in deriving Eq. (36) we have assigned the same asymmetry parameter (denoted x) to the counting fields and to the affinities. We could choose a different asymmetry parameter for the counting fields and for the affinities, and rewrite Eq. (36) in a general form

$$\mathcal{F}_G(\lambda,\lambda_P,\mathcal{A},\mathcal{A}_P;B,x,y) \equiv \mathcal{F}_G([1+y]\lambda,y\lambda,\lambda_P,[1+x]\mathcal{A},x\mathcal{A},\mathcal{A}_P;B). \tag{C4}$$

Similarly to Eq. (46), the transport coefficients in the present scheme are given by

$$L^{j\ell}_{km}(B,x,y) \equiv \left.\frac{\partial^{j+k+\ell+m}\mathcal{F}_G(\lambda,\lambda_P,\mathcal{A},\mathcal{A}_P;B,x,y)}{\partial\lambda^j\partial\mathcal{A}^k\partial\lambda_P^\ell\partial\mathcal{A}_P^m}\right|_{\lambda=\lambda_P=\mathcal{A}=\mathcal{A}_P=0}. \tag{C5}$$

These transport coefficients are related to the heat conductance matrix Eq. (C2) via

$$\begin{aligned} L^{10}_{10}(B,x,y) =& K_{LL} + (K_{LL}+K_{RL})\,y + (K_{LL}+K_{LR})\,x \\ &+ (K_{LL}+K_{LR}+K_{RL}+K_{RR})\,xy, \\ L^{10}_{01}(B,x,y) =& K_{LP} + (K_{LP}+K_{RP})\,y, \\ L^{01}_{10}(B,x,y) =& K_{PL} + (K_{PL}+K_{PR})\,x, \\ L^{01}_{01}(B,x,y) =& K_{PP}. \end{aligned} \tag{C6}$$

In the minimal-correlation coordinate approach, one chooses y as [20]

$$y = -\frac{K_{LP}}{K_{LP}+K_{RP}}. \tag{C7}$$

Then, from the second of Eqs. (C6),

$$L^{10}_{01}[B;-K_{LP}/(K_{LP}+K_{RP})] = 0. \tag{C8}$$

This choice removes many of the vertex corrections discussed in Sec. III B (see Figs. 3, 4, and 5 there). In particular, for the linear transport case, vertex corrections vanish (Fig. 3).

APPENDIX D: THE THIRD CUMULANT OF THE TWO-TERMINAL JUNCTION

The third derivative of $\mathcal{F}$, the CGF of the effective two-terminal junction, is obtained by taking the complete derivative of Eq. (53) and exploiting Eq. (49). We find $(\gamma,\gamma',\gamma''=c,q)$

$$\begin{aligned} \frac{d^3\mathcal{F}}{da_{\gamma''}\,da_{\gamma'}\,da_\gamma} =& \frac{\partial^3\mathcal{F}_G}{\partial a_{\gamma''}\,\partial a_{\gamma'}\,\partial a_\gamma} \\ &+ \sum_{\alpha,\alpha'=c,q} \frac{\partial^3\mathcal{F}_G}{\partial a_{\gamma''}\,\partial a_{\gamma'}\,\partial v_\alpha} U_{\alpha\alpha'} \frac{\partial^2\mathcal{F}_G}{\partial a_\gamma\,\partial v_{\alpha'}} + \frac{\partial^2\mathcal{F}_G}{\partial a_{\gamma'}\,\partial v_\alpha}\frac{\partial U_{\alpha\alpha'}}{\partial a_{\gamma''}}\frac{\partial^2\mathcal{F}_G}{\partial a_\gamma\,\partial v_{\alpha'}} + \frac{\partial^2\mathcal{F}_G}{\partial a_{\gamma'}\,\partial v_\alpha} U_{\alpha\alpha'} \frac{\partial^3\mathcal{F}_G}{\partial a_{\gamma''}\,\partial a_\gamma\,\partial v_{\alpha'}} \\ &+ \sum_{\beta,\beta'=c,q} \frac{\partial^2\mathcal{F}_G}{\partial a_{\gamma''}\partial v_{\beta'}} U_{\beta'\beta} \left\{ \frac{\partial^3\mathcal{F}_G}{\partial a_{\gamma'}\,\partial a_\gamma\,\partial v_\beta} \right. \\ &\left. + \sum_{\alpha,\alpha'=c,q} \left[\frac{\partial^3\mathcal{F}_G}{\partial a_{\gamma'}\,\partial v_\beta\,\partial v_\alpha} U_{\alpha\alpha'} \frac{\partial^2\mathcal{F}_G}{\partial a_\gamma\,\partial v_{\alpha'}} + \frac{\partial^2\mathcal{F}_G}{\partial a_{\gamma'}\,\partial v_\alpha}\frac{\partial U_{\alpha\alpha'}}{\partial v_\beta}\frac{\partial^2\mathcal{F}_G}{\partial a_\gamma\,\partial v_{\alpha'}} + \frac{\partial^2\mathcal{F}_G}{\partial a_{\gamma'}\,\partial v_\alpha} U_{\alpha\alpha'} \frac{\partial^3\mathcal{F}_G}{\partial a_\gamma\,\partial v_\beta\,\partial v_{\alpha'}} \right] \right\} \\ =& \frac{\partial^3\mathcal{F}_G}{\partial a_{\gamma''}\partial a_{\gamma'}\partial a_\gamma} + \sum_{\{i,j,k\}} \sum_{\alpha,\alpha'=c,q} \frac{\partial^2\mathcal{F}_G}{\partial a_i\partial v_{\alpha'}} U_{\alpha'\alpha} \frac{\partial^3\mathcal{F}_G}{\partial a_j\partial a_k\partial v_\alpha} \\ &+ \sum_{\{i,j,k\}} \sum_{\alpha_1,\alpha_2,\alpha_1',\alpha_2'=c,q} \frac{\partial^2\mathcal{F}_G}{\partial a_i\partial v_{\alpha_1'}} U_{\alpha_1'\alpha_1} \frac{\partial^2\mathcal{F}_G}{\partial a_j\partial v_{\alpha_2'}} U_{\alpha_2'\alpha_2} \frac{\partial^2\mathcal{F}_G}{\partial a_k\partial v_{\alpha_1}\partial v_{\alpha_2}} \\ &+ \sum_{\alpha_1,\alpha_2,\alpha_3,\alpha_1',\alpha_2',\alpha_3'=c,q} \frac{\partial^2\mathcal{F}_G}{\partial a_\gamma\partial v_{\alpha_1'}} U_{\alpha_1'\alpha_1} \frac{\partial^2\mathcal{F}_G}{\partial a_{\gamma'}\partial v_{\alpha_2'}} U_{\alpha_2'\alpha_2} \frac{\partial^2\mathcal{F}_G}{\partial a_{\gamma''}\partial v_{\alpha_3'}} U_{\alpha_3'\alpha_3} \frac{\partial^3\mathcal{F}_G}{\partial v_{\alpha_1}\partial v_{\alpha_2}\partial v_{\alpha_3}}, \end{aligned} \tag{D1}$$

where we have used Eqs. (51). Here $\sum_{\{i,j,k\}}$ means summation over the three cyclic combinations of $\{\gamma,\gamma',\gamma''\}$.

APPENDIX E: THE SYMMETRIC AND ANTISYMMETRIC COMPONENTS OF THE NOISE WITH RESPECT TO A MAGNETIC FIELD

As is explained in the main text, the full expression for the linear-response noise (see Fig. 5) turns out to be rather cumbersome. However, it is possible to obtained certain relations among its symmetric and antisymmetric components, with respect to the magnetic field.

The symmetric component is

$$\begin{aligned} L^{1}_{2,+} = L^{2}_{1,+} = L^{20}_{10,+} &+ 2\,\frac{L^{10}_{01,+}\left(L^{20}_{01,+} - 4L^{10}_{11,+}\right) - L^{10}_{01,-}\left(L^{01}_{20,-} - 2L^{10}_{11,-}\right)}{L^{02}_{00,+}} \\ &+ 4\,\frac{\left(L^{10}_{01,+}\right)^2\left(L^{02}_{10,+} + 2L^{11}_{01,+}\right) - \left(L^{10}_{01,-}\right)^2 L^{02}_{10,+} - 2L^{10}_{01,+}L^{10}_{01,-}L^{10}_{02,-}}{\left(L^{02}_{00,+}\right)^2} \\ &- 8\,\frac{\left[\left(L^{10}_{01,-}\right)^2 - \left(L^{10}_{01,+}\right)^2\right]\left(L^{10}_{01,-}L^{01}_{02,-} - L^{10}_{01,+}L^{02}_{01,+}\right)}{\left(L^{02}_{00,+}\right)^3}, \end{aligned} \tag{E1}$$

and the asymmetric component is

$$\begin{aligned} L^{1}_{2,-} = L^{2}_{1,-}/3 = L^{10}_{20,-} &+ 2\,\frac{L^{10}_{01,-}L^{20}_{01,+} - L^{10}_{01,+}\left(L^{01}_{20,-} + 2L^{10}_{11,-}\right)}{L^{02}_{00,+}} \\ &+ 4\,\frac{2\left[\left(L^{10}_{01,+}\right)^2 - \left(L^{10}_{01,-}\right)^2\right]L^{01}_{11,-} + \left[\left(L^{10}_{01,+}\right)^2 + \left(L^{10}_{01,-}\right)^2\right]L^{10}_{02,-} - 2L^{10}_{01,-}L^{10}_{01,+}L^{11}_{01,+}}{\left(L^{02}_{00,+}\right)^2} \\ &- 8\,\frac{\left[\left(L^{10}_{01,-}\right)^2 - \left(L^{10}_{01,+}\right)^2\right]\left(L^{10}_{01,-}L^{02}_{01,+} - L^{10}_{01,+}L^{01}_{02,-}\right)}{\left(L^{02}_{00,+}\right)^3}. \end{aligned} \tag{E2}$$

[1] R. Sánchez and M. Büttiker, Europhys. Lett. **100**, 47008 (2012); **104**, 49901 (2013).

[2] F. Giazotto, T. T. Heikkilä, A. Luukanen, A. M. Savin, and J. P. Pekola, Rev. Mod. Phys. **78**, 217 (2006).

[3] L. W. Molenkamp, H. van Houten, C. W. J. Beenakker, R. Eppenga, and C. T. Foxon, Phys. Rev. Lett. **65**, 1052 (1990).

[4] S. Möller, H. Buhmann, S. F. Godijn, and L. W. Molenkamp, Phys. Rev. Lett. **81**, 5197 (1998); S. F. Godijn, S. Möller, H. Buhmann, L. W. Molenkamp, and S. A. van Langen, *ibid.* **82**, 2927 (1999).

[5] V. Venkatachalam, S. Hart, L. Pfeiffer, K. West, and A. Yacoby, Nat. Phys. **8**, 676 (2012).

[6] J. Matthews, F. Battista, D. Sanchez, P. Samuelsson, and H. Linke, arXiv:1306.3694.

[7] R. Sánchez and M. Büttiker, Phys. Rev. B **83**, 085428 (2011); B. Sothmann, R. Sánchez, A. N. Jordan, and M. Büttiker, *ibid.* **85**, 205301 (2012); A. N. Jordan, B. Sothmann, R. Sánchez, and M. Büttiker, *ibid.* **87**, 075312 (2013); B. Sothmann, R. Sánchez, A. N. Jordan, and M. Büttiker, New J. Phys. **15**, 095021 (2013); R. Sánchez, B. Sothmann, A. N. Jordan, and M. Büttiker, *ibid.* **15**, 125001 (2013).

[8] O. Entin-Wohlman, Y. Imry, and A. Aharony, Phys. Rev. B **82**, 115314 (2010).

[9] D. Sánchez and L. Serra, Phys. Rev. B **84**, 201307(R) (2011).

[10] K. Saito, G. Benenti, G. Casati, and T. Prosen, Phys. Rev. B **84**, 201306(R) (2011).

[11] K. Brandner, K. Saito, and U. Seifert, Phys. Rev. Lett. **110**, 070603 (2013).

[12] R. López and D. Sánchez, Phys. Rev. B **88**, 045129 (2013).

[13] D. Sánchez and R. López, Phys. Rev. Lett. **110**, 026804 (2013).

[14] S. F. Svensson, E. A. Hoffmann, N. Nakpathomkun, P. M. Wu, H. Xu, H. A. Nilsson, D. Sanchez, V. Kashcheyevs, and H. Linke, New J. Phys. **15**, 105011 (2013); S. Hwang, D. Sánchez, M. Lee, and R. López, *ibid.* **15**, 105012 (2013).

[15] H.-L. Engquist and P. W. Anderson, Phys. Rev. B **24**, 1151 (1981).

[16] U. Sivan and Y. Imry, Phys. Rev. B **33**, 551 (1986).

[17] L. S. Levitov and G. B. Lesovik, JETP Lett. **58**, 230 (1993) ; L. S. Levitov, H. Lee, and G. B. Lesovik, J. Math. Phys. **37**, 4845 (1996).

[18] *Quantum Noise in Mesoscopic Physics*, NATO Science Series II: Mathematics, Physics and Chemistry Vol. 97, edited by Yu. V. Nazarov (Kluwer Academic, Dordrecht, 2003).

[19] S. Pilgram, A. N. Jordan, E. V. Sukhorukov, and M. Büttiker, Phys. Rev. Lett. **90**, 206801 (2003).

[20] A. N. Jordan, E. V. Sukhorukov, and S. Pilgram, J. Math. Phys. **45**, 4386 (2004).

[21] S. Pilgram, P. Samuelsson, H. Förster, and M. Büttiker, Phys. Rev. Lett. **97**, 066801 (2006).

[22] H. Förster, P. Samuelsson, and M. Büttiker, New J. Phys. **9**, 117 (2007); H. Förster, P. Samuelsson, S. Pilgram, and M. Büttiker, Phys. Rev. B **75**, 035340 (2007).

[23] T. T. Heikkilä and Yu. V. Nazarov, Phys. Rev. Lett. **102**, 130605 (2009).
[24] M. A. Laakso, T. T. Heikkilä, and Yu. V. Nazarov, Phys. Rev. Lett. **104**, 196805 (2010); Phys. Rev. B **82**, 205316 (2010); **85**, 184521 (2012); Phys. Rev. Lett. **108**, 067002 (2012).
[25] D. Golubev, T. Faivre, and J. P. Pekola, Phys. Rev. B **87**, 094522 (2013).
[26] D. J. Evans, E. G. D. Cohen, and G. P. Morriss, Phys. Rev. Lett. **71**, 2401 (1993); **71**, 3616 (1993); G. Gallavotti and E. G. D. Cohen, *ibid.* **74**, 2694 (1995); G. Gallavotti, *ibid.* **77**, 4334 (1996).
[27] J. Tobiska and Yu. V. Nazarov, Phys. Rev. B **72**, 235328 (2005).
[28] H. Förster and M. Büttiker, Phys. Rev. Lett. **101**, 136805 (2008).
[29] H. Förster and M Büttiker, unpublished (arXiv:0805.0362v2).
[30] K. Saito and Y. Utsumi, Phys. Rev. B **78**, 115429 (2008).
[31] D. Andrieux, P. Gaspard, T. Monnai, and S. Tasaki, New J. Phys. **11**, 043014 (2009).
[32] M. Esposito, U. Harbola, and S. Mukamel, Rev. Mod. Phys. **81**, 1665 (2009).
[33] M. Campisi, P. Hänggi, and M. Talkner, Rev. Mod. Phys. **83**, 771 (2011).
[34] A. Altland, A. De Martino, R. Egger, and B. Narozhny, Phys. Rev. Lett. **105**, 170601 (2010); Phys. Rev. B **82**, 115323 (2010).
[35] R. Lopez, J. S. Lim, and D. Sanchez, Phys. Rev. Lett. **108**, 246603 (2012); R. Sanchez, R. Lopez, D. Sanchez, and M. Büttiker, *ibid.* **104**, 076801 (2010); J. S. Lim, D. Sanchez, and R. Lopez, Phys. Rev. B **81**, 155323 (2010); D. Sanchez, *ibid.* **79**, 045305 (2009).
[36] Y. Utsumi, D. S. Golubev, M. Marthaler, K. Saito, T. Fujisawa, and G. Schön, Phys. Rev. B **81**, 125331 (2010).
[37] B. Küng, C. Rössler, M. Beck, M. Marthaler, D. S. Golubev, Y. Utsumi, T. Ihn, and K. Ensslin, Phys. Rev. X **2**, 011001 (2012); J. Appl. Phys. **113**, 136507 (2013).
[38] S. Nakamura, Y. Yamauchi, M. Hashisaka, K. Chida, K. Kobayashi, T. Ono, R. Leturcq, K. Ensslin, K. Saito, Y. Utsumi, and A. C. Gossard, Phys. Rev. Lett. **104**, 080602 (2010); Phys. Rev. B **83**, 155431 (2011).
[39] Y. Utsumi and K. Saito, Phys. Rev. B. **79**, 235311 (2009).
[40] O.-P. Saira, Y. Yoon, T. Tanttu, M. Möttönen, D. V. Averin, and J. P. Pekola, Phys. Rev. Lett. **109**, 180601 (2012); J. V. Koski, T. Sagawa, O.-P. Saira, Y. Yoon, A. Kutvonen, P. Solinas, M. Möttönen, T. Ala-Nissila, and J. P. Pekola, Nat. Phys. **9**, 644 (2013); J. V. Koski, V. F. Maisi, J. P. Pekola, and D. V. Averin, arXiv:1402.5907.
[41] C. Jarzynski and D. K. Wójcik, Phys. Rev. Lett. **92**, 230602 (2004).
[42] K. Saito and A. Dhar, Phys. Rev. Lett. **99**, 180601 (2007).
[43] B. K. Agarwalla, H. Li, B. Li, and J.-S. Wang, Phys. Rev. E **89**, 052101 (2014).
[44] S. Bedkihal, M. Bandyopadhyay, and D. Segal, Eur. Phys. J. B **506**, 86 (2013).
[45] Note the sign convention for the currents. It differs from the one commonly used in treatments of irreversible thermodynamics; see, e.g., H. B. Callen, *Thermodynamics and an Introduction to Thermostatistics*, 2nd ed. (Wiley, New York, 1985).
[46] M. Büttiker, IBM J. Res. Dev. **32**, 317 (1988).
[47] M. Kindermann and S. Pilgram, Phys. Rev. B **69**, 155334 (2004).
[48] K. Kanazawa, T. Sagawa, and H. Hayakawa, Phys. Rev. Lett. **108**, 210601 (2012); Phys. Rev. E **87**, 052124 (2013); T. G. Sano and H. Hayakawa, *ibid.* **89**, 032104 (2014).
[49] A. Kamenev, *Field Theory of Nonequilibrium Systems* (Cambridge University Press, Cambridge, 2011).
[50] D. S. Golubev, Y. Utsumi, M. Marthaler, and G. Schön, Phys. Rev. B **84**, 075323 (2011).
[51] C. Jarzynski, J. Stat. Phys. **98**, 77 (2000).
[52] Y. Utsumi, D. S. Golubev, M. Marthaler, G. Schön, and K. Kobayashi, Phys. Rev. B **86**, 075420 (2012).
[53] Note, though, that the problem considered here is somewhat simpler, since the dynamics of the classical variable, i.e., the energy of the probe, is not governed by a Hamiltonian.
[54] H. Touchette, Phys. Rep. **478**, 1 (2009).
[55] G. Baym and L. P. Kadanoff, Phys. Rev. **124**, 287 (1961); G. Baym, *ibid.* **127**, 1391 (1962).
[56] Y. Utsumi, O. Entin-Wohlman, A. Ueda, and A. Aharony, Phys. Rev. B **87**, 115407 (2013).
[57] K. E. Nagaev, Phys. Rev. B **66**, 075334 (2002); K. E. Nagaev, P. Samuelsson, and S. Pilgram, *ibid.* **66**, 195318 (2002).